COMMUNICATIONS CHEMISTRY

ARTICLE

DOI: 10.1038/s42004-018-0012-4 OPEN

Directly converting carbon dioxide to linear α-olefins on bio-promoted catalysts

Lisheng Guo[1,2], Jian Sun[1], Xuewei Ji[1,2], Jian Wei[1,2], Zhiyong Wen[1,2], Ruwei Yao[1,2], Hengyong Xu[1] & Qingjie Ge[1]

Although considerable efforts have been made in converting carbon dioxide to hydrocarbons via hydrogenation processes, precise control of C–C coupling towards heavy olefins remains a challenge. Here we report a carbon dioxide hydrogenation to olefin process that achieves 72% selectivity for alkenes and 50.3% selectivity for C_{4-18} alkenes, of which formation of linear α-olefins accounts for 80%. The process is catalyzed by carbon-supported iron, commonly used in C–C coupling reactions, with multiple alkali promoters extracted from corncob. The design is based on the synergistic catalysis of mineral elements in biomass enzyme on which carbon dioxide can be directly converted into carbohydrate. The mineral elements from corncob may promote the surface enrichment of potassium, suppressing the secondary hydrogenation of alkenes on active sites. Furthermore, carburization of iron species is enhanced to form more Fe_5C_2 species, promoting both the reverse water–gas shift reaction and subsequent C–C coupling.

[1] Dalian National Laboratory for Clean Energy, Dalian Institute of Chemical Physics, Chinese Academy of Sciences, Dalian 116023, China. [2] University of Chinese Academy of Sciences, Beijing 100049, China. Correspondence and requests for materials should be addressed to J.S. (email: sunj@dicp.ac.cn) or to Q.G. (email: geqj@dicp.ac.cn)

Converting carbon dioxide (CO_2) to valuable commodity chemicals is a potential route to mitigate the detrimental effects associated with anthropogenic CO_2 emissions, and may benefit energy carrier technology and chemical production[1, 2]. Among common CO_2 transformation pathways comprising photocatalytic conversion, electrochemical reduction, catalytic hydrogenation, and other related processes, CO_2 hydrogenation to hydrocarbons via reverse water-gas shift (RWGS) reaction followed by C–C coupling has been deemed as one of the most promising means of CO_2 utilization over the last two decades[3–5].

Generally, light hydrocarbons with less than four carbon numbers, especially methane, are the major hydrocarbon products in the process of CO_2 hydrogenation. The addition of alkali metal ions to iron catalysts can increase the selectivity for light olefins during CO_2 or CO hydrogenation. The addition of alkali promoters results in a decrease in H_2 adsorption and an increase in CO_2 adsorption, significantly enhancing production of light olefins[6, 7]. It is reported that alkali (K and Na)-promoted Fe-based catalysts exhibit excellent selectivity exceeding 45% for light olefins[8, 9].

In addition to lower olefins, higher olefins and in particular linear α-olefins (LAOs), which contain a terminal carbon–carbon double bond, are important and expensive industrial feedstocks for producing highly value-added chemicals, such as lubricants, detergents, and polyolefins[10, 11]. Currently, heavy α-olefins with carbon number higher than four are generally produced via oligomerization of ethylene mostly produced from petroleum resources[12–14]. Recently, Zhai et al.[15] reported a Na and Zn modified Fe_5C_2 catalyst applied to Fischer–Tropsch synthesis (FTS) which delivered high selectivity for C_{5+} alkenes and particularly LAO. No related reports concerning LAO production from CO_2 have been reported to our knowledge, in spite of the fact that CO_2 conversion to heavy hydrocarbons has been demonstrated in recent years[16–18].

Precise control of carbon chain growth to achieve a high selectivity for heavy hydrocarbons with a desired carbon range or bonding pattern (saturated, unsaturated, branched, etc.) remains a severe challenge that limits selective conversion of CO_2. In contrast to CO hydrogenation, CO_2 as a thermodynamically stable molecule needs an initial reduction to a CO intermediate and then subsequent C–C coupling. This requires active sites matching both RWGS and C–C coupling. Thus, these challenges make CO_2 hydrogenation to heavy hydrocarbons more difficult than FTS. Very recently, two multifunctional catalysts (Na-Fe_3O_4/HZSM-5 (ref. [19]) and In_2O_3/HZSM-5 (ref. [20])) were reported, which can selectively convert CO_2 to gasoline-ranged hydrocarbons with selectivity of more than 78% in all hydrocarbons.

CO_2 in nature can be efficiently converted into carbohydrates via biological photosynthesis over enzymes in biomass. Biomass as a renewable resource contains many mineral elements, such as K, Mg, Ca, and Si, which are involved in carbohydrate synthesis from CO_2 conversion. Such mineral elements in biomass form an optimal composition ratio match with the evolution of plants, and promote enzymes to exhibit high-performance biocatalysis. The introduction of mineral elements from biomass, i.e. corncob (CC), is a promising alternative to the use of chemical promoter sources. These environmental friendly resources have been named as biopromoters[21].

Herein, we design an enzyme-like integrated catalyst comprising iron carbides and alkali promoters from calcined CC ash, accomplishing direct conversion of CO_2 hydrogenation into LAO with a selectivity in hydrocarbons of higher than 40% and a total olefin selectivity in hydrocarbons of 72%. In this "CO_2-LAO" reaction the product selectivity approached that of FTS[15]. Compared to unpromoted and chemically promoted iron-based catalysts, the biopromoter modified iron catalysts are demonstrated to have a synergetic effect for improving the performance of CO_2 hydrogenation.

Results

Composition of the bio-promoted Fe catalyst. The corresponding contents of K, Mg, Ca, and Si in the prepared CC ash were 22.8 wt%, 21.8 wt%, 7.2 wt%, and 2.1 wt%, respectively, and the remaining elements were O and other trace elements accounting for 46.1 wt% (Supplementary Table 1). The main phases of K, Mg, Ca, and Si are ascribed to KCl, MgO, $CaCO_3$, and SiO_2, respectively (Supplementary Fig. 1). The single mineral promoter, simulated four promoters, and biopromoters were added into the Fe/C catalyst by a facile physical mixing method, marked as Fe/C-M, Fe/C-Chem, and Fe/C-Bio respectively, and the loading of iron in these catalysts ranged from 14.0% to 16.4% (Supplementary Table 2). The morphology of fresh Fe/C-Bio existed in the form of spherical structure with a diameter of 3–5 μm, and Fe, K, Ca, and Mg promoters were uniformly distributed in the catalyst system (Supplementary Fig. 2). Carbonaceous spheres as promising supports possess excellent features, such as facilitated the formation of iron carbides during H_2 activation and suppressed the aggregation of nanoparticles during reaction processes[22, 23].

Catalytic performance in the CO_2–LAO reaction. The performance of CO_2 hydrogenation on prepared catalysts with a suitable additive amount was evaluated under optimal reaction conditions (Table 1 and Supplementary Fig. 3). C_{4-18} alkenes selectivity was sharply increased from 11.6 to 50.3%, and methane selectivity was suppressed simultaneously from 39.2 to 11.8% when biopromoters were added into the Fe/C catalyst. It is

Table 1 The catalytic performance of CO_2–LAO over various catalysts

Cat.	Conv. (%)	CO sel. (%)	Hydrocarbons sel. (%)			Alkenes sel. (%)		LAO/O[a](%)	α[b]
			CH_4	C_{2-3}	C_{4-18}	$C_{4-18}^{=}$	$C_{2-18}^{=}$		
Fe/C	25	22.2	39.2	34.4	26.4	11.6	21.2	3.4	0.53
Fe/C-Bio	31	23.2	11.8	24.4	63.8	50.3	72.0	80	0.72
Fe/C-Chem	24	36.2	26.7	39.8	33.5	24.8	53.1	73	0.57
Fe/C-K	28	22.6	24.0	38.1	37.9	30.5	60.4	75	0.53
Fe/C-Ca	25	31.9	29.0	37.0	34.0	13.7	24.3	42	0.55
Fe/C-Mg	26	28.5	33.2	35.2	31.6	14.9	27.0	42	0.56
Fe/C-Si	22	28.0	43.1	36.6	20.3	5.7	12.9	56	0.54

All the conversion and selectivity data are collected at a stable 4–6 h on stream. Reaction conditions: 320 °C, 1.0 MPa, $H_2/CO_2 = 3:1$, $W/F = 10$ g h mol^{-1}, additive amount of biopromoters is 15 wt% (mass ratio of biopromoters to Fe/C)
[a] The ratio of linear α-$C_{4-18}^{=}/C_{4-18}^{=}$, LAO stands for linear α-C_{4-18} alkenes. The additive amount of K, Mg, Ca, and Si is equal to that in the Fe/C-Bio
[b] The value of α is calculated based on C_{3-10} products

noteworthy that LAO selectivity accounts for 80% in C_{4-18} alkenes and LAO is mainly concentrated on the carbon number range of 4 to 9, which is beneficial to the production of lubricating oil and plasticizer. Compared to the selectivity of C_{4-18} alkenes over conventional iron-based catalysts, the C_{4-18} alkenes selectivity over biopromoters-modified iron catalysts reaches maximum value in reported literatures (Supplementary Table 3). Besides that, all the Fe/C, bio-promoted, and chem-promoted Fe/C catalysts show stable catalytic performance in a 6 h reaction (Supplementary Fig. 4). A long-time stability test of 100 h for the Fe/C-Bio shows that the conversion of CO_2 remains unchanged, as well as the selectivity to CH_4, C_{5+}, and LAO (Supplementary Fig. 5); therefore, it indicates that bio-promoted iron-based catalysts are stable and efficient for heavy olefins production especially for LAO. More interestingly, we also find similar results after replacing the feedstock from the mixture of CO_2 and H_2 by that of CO and H_2 (Supplementary Table 4). After biopromoters are physically introduced, the CO conversion and LAO selectivity in C_{4-18} alkenes are both evidently promoted to 85% (vs 49% for the Fe/C) and 67% (vs 41% for the Fe/C) under the same catalytic conditions (280 °C, 1.0 MPa, $H_2/CO = 1:1$), respectively. Furthermore, a very high total olefin selectivity of 78.4% as well as a high conversion of 95% is observed after the temperature is lifted to 320 °C, which is the same temperature as CO_2 hydrogenation.

To verify the biopromoter effect and explain the superior selectivity of linear olefins, each separated promoter addition experiment was also carried out (Table 1). The CO_2–LAO performance was improved when the K, Mg, and Ca was alone added to unpromoted Fe/C, among which the promotional effect of K was most obvious in terms of enhancing olefins selectivity (21.2–60.4%). The potassium promoter not only is beneficial to the RWGS reaction (enhanced CO_2 conversion) but also enhances selective C–C coupling to olefin (enhanced heavy olefin selectivity). To further investigate the effect of K promoter, the biopromoters were washed with deionized water for several times and then subsequently added into Fe/C (noted as Fe/C-Bio-W). The content of light hydrocarbons (including C_{1-3}) is increased while CO_2 conversion is decreased after soluble KCl was removed (Supplementary Tables 1 and 5). It indicates that soluble and insoluble K salts are both essential for improving the selectivity of heavy olefins. In addition, the doping of basic Mg and Ca promoter results in a small increase in terms of higher olefins selectivity. In view of the promoting effect between S and alkali metal[24], the doping of alkali metals and S element was also tested in reaction conditions (Supplementary Table 6). The existence of few S element introduced by physical mixing did not improve the olefins selectivity. K as a key ingredient mainly suppresses methanation reaction of CO_2 and increases the activity of C–C coupling[25], and the addition of Mg and Ca also suppresses the formation of methane as well as enhances the selectivity to olefins during the process of C–C coupling[26]. Yet for Fe/C-Chem, C_{4-18} alkenes selectivity is only half of those on Fe/C-Bio. These findings indicate that the higher selectivity of C_{4-18} alkenes obtained from Fe/C-Bio is difficult to be simulated by the doping of chemical promoters, suggesting that biopromoters, rather than chemical promoters, induce unique synergistic promoting effect.

Chemical state of catalytic active phases. X-ray diffraction (XRD) measurements were used to determine the species phases of catalysts. According to the characteristic diffraction peaks data of KCl (JCPDS, 41-1476), XRD pattern of Fe/C-Bio and Fe/C-Chem shows the existence of K promoter (Fig. 1). The diffraction patterns of MgO and $CaCO_3$ were not detected in Fe/C-Bio owing to the low content in the catalysts. Other than used Fe/C and Fe/C-Chem, additional peaks of Fe_5C_2 were clearly observed in the used Fe/C-Bio, indicating more Fe_5C_2 formation with the addition of biopromoters. Besides, the peaks of Fe_5C_2 can be also obviously distinguished after 100 h reaction. The existence of more Fe_5C_2 is beneficial to the enhancement of C–C coupling and suppressing of methane formation[27, 28]. Finally, iron oxides and iron carbides will achieve well matching of RWGS reaction (Eq. (1)) and subsequent C–C coupling (Eq. (2)), improving the activity of CO_2 hydrogenation as well as the selectivity of heavy

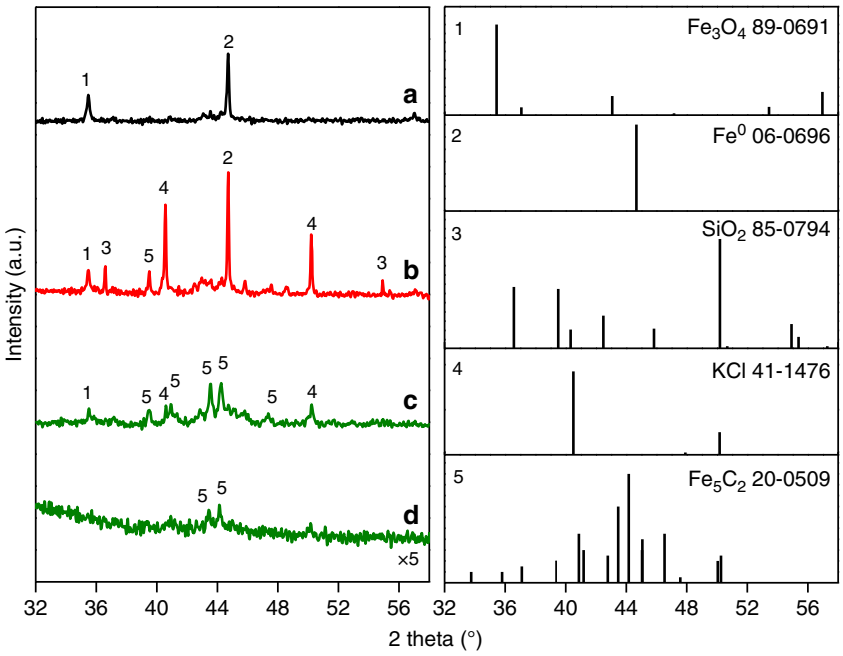

Fig. 1 XRD patterns of various used catalysts. The Fe/C (**a**), Fe/C-Chem (**b**), and Fe/C-Bio (**c**) are derived after catalytic reaction for 6 h. (**d**) Fe/C-Bio catalyst after catalytic reaction for 100 h

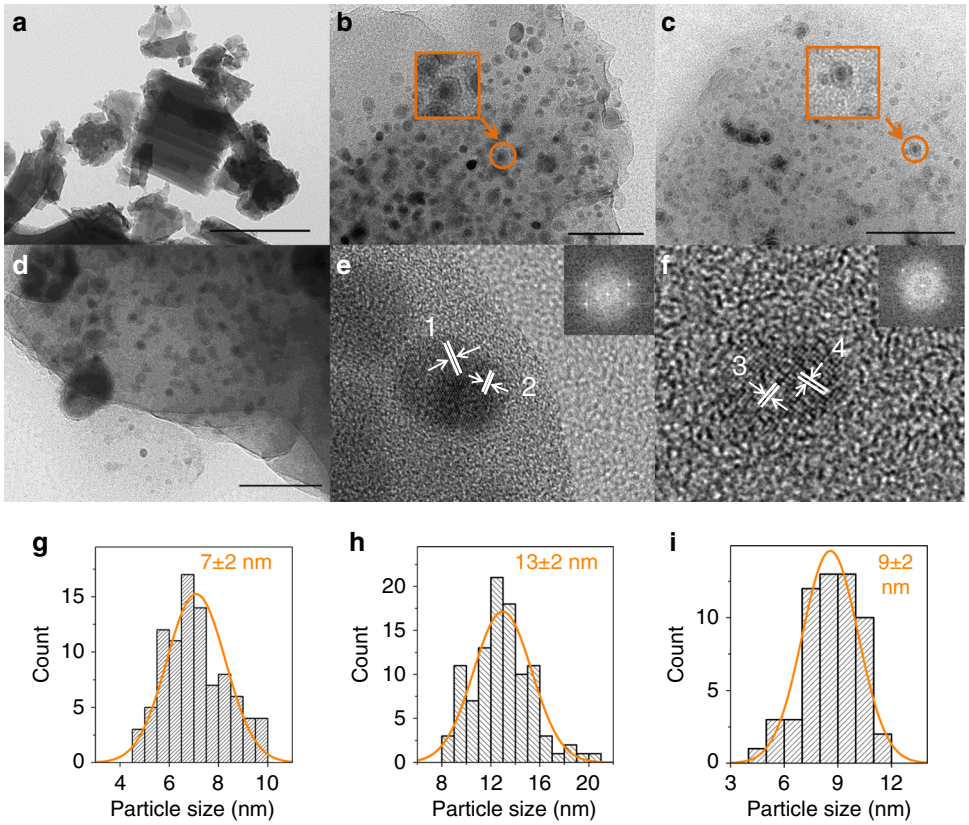

Fig. 2 TEM images of catalysts. **a** Fresh Fe/C-Bio. **b** Fe/C-Chem used for 6 h. **c** Fe/C-Bio used for 6 h. **d** Fe/C-Bio used for 100 h. The lattice spacing 1 (or 2) of 2.96 Å corresponds to Fe_3O_4 (220). **e** High-resolution TEM images of Fe/C-Chem used for 6 h. The lattice spacing 3 of 2.50 Å and lattice spacing 4 of 2.93 Å corresponds to Fe_5C_2 (002) and Fe_5C_2 (310), respectively. **f** High-resolution TEM images of Fe/C-Bio used for 6 h. **g** Particle distribution of panel **c**. **h** Particle distribution of panel **b**. **i** Particle distribution of panel **d**. The scale bar for panel **a**, 500 nm. The scale bar for panels **b**–**d**, 100 nm

hydrocarbons.

$$CO_2 + H_2 \rightarrow CO + H_2O \quad (1)$$

$$CO + 2H_2 \rightarrow -CH_2 - + H_2O \quad (2)$$

For the used Fe/C, the main phases were Fe^0 and Fe_3O_4 rather than Fe_5C_2, showing an inferior selectivity of heavy hydrocarbons. Fe^0 and Fe_3O_4 existed in Fe/C-Chem were also main phases, and presented a higher selectivity of alkenes compared to Fe/C owing to the promotion effect of alkali metal.

Transmission electron microscope (TEM) was applied to determine the distribution and size of iron species (Fig. 2). After reaction, Fe/C-Bio exhibited uniform particles distribution of iron species while fresh Fe/C-Bio consisted of irregular large particles. The precursor of iron species contains a large number of humboldtine ($FeC_2O_4{\cdot}2H_2O$, JCPDS 23-0293) in carbonaceous spheres (Supplementary Fig. 6)[21]. The decomposition of humboldtine under H_2 condition presented magnetite, iron carbides, and metal Fe[29]. The decomposed metal Fe acts with CO_2 and H_2 to form active sites of RWGS and C–C coupling, and then converts CO_2 and H_2 into hydrocarbons[1]. Therefore, no additional calcination is needed in our work, which is different from conventional preparation processes.

The difference between structure shape and size of iron particles result from humboldtine decomposition and subsequent reaction with CO_2 and H_2. The statistical result of particles shows that Fe/C-Bio particle size after 6 and 100 h mainly distribute on the range of 5–9 nm (Fig. 2g) and 7–11 nm (Fig. 2i), respectively, which is beneficial to maintain a low CH_4 selectivity and high light olefins selectivity for CO hydrogenation due to the reported particle size effect[30]. However, the particle size distribution of used Fe/C-Chem was centered on 11–15 nm (Fig. 2h), which is much larger than that of Fe/C-Bio. Well size distribution of particles is vital for the activity and selectivity of catalytic performance, thus small average particle size change of iron species from 7 to 9 nm is favorable for maintaining the catalytic performance of catalyst during stability test (Fig. 2c and Supplementary Fig. 5). Besides particle size, the main active phases are different between Fe/C-Chem and Fe/C-Bio as further verified by high-resolution TEM (HR-TEM). The lattice planes of Fe_5C_2 (002) and (210) are detected as main active phase for Fe/C-Bio (Fig. 2f) while Fe_3O_4 (220) is present for Fe/C-Chem (Fig. 2e), well consistent with XRD analysis. In Fig. 2b, iron species of Fe/C-Chem presented a core-shell structure, and the core of Fe_3O_4 and Fe was encapsulated by a shell of amorphous carbon[31]. As for Fe/C-Bio, iron species were mainly isolated Fe_5C_2 nanoparticles without similar core-shell structure. These findings indicate that biopromoters are conducive to the carburization of Fe_3O_4 and Fe core with amorphous carbon shell, producing small particles of active phases and providing more contact interfaces between active sites and feed gas.

Formation and nature of catalytic active phases. Fe species in these promoted catalysts are more easily reduced. In Supplementary Fig. 7, the H_2-TPR curves of Fe/C, Fe/C-Bio, and Fe/C-Chem are presented. In heating conditions under an H_2 atmosphere, the decomposition of humboldtine, a precursor for active iron species prepared by the hydrothermal process, will produces magnetite, iron carbides and metal Fe with an obvious

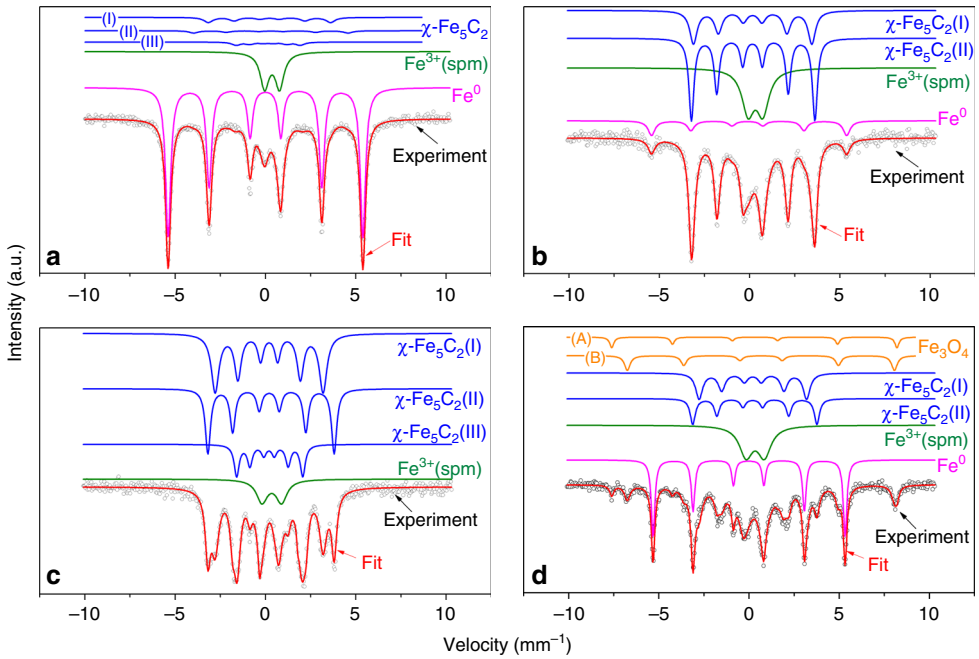

Fig. 3 ^{57}Fe Mössbauer spectra of various catalysts. **a** Reduced Fe/C, **b** reduced Fe/C-Bio, **c** used Fe/C-Bio, and **d** used Fe/C-Chem. In each panel, the black scatter curve stands for the experiment data, and the red line stands for the calculated data by fitted. Data analyses were performed assuming a Lorentzian line-shape for computer folding and fitting. The components of iron phases were identified based on the Mössbauer parameters including isomer shift, quadruple splitting, and magnetic hyperfine field

H_2 consumption peak (450 °C for Fe/C) in the H_2-TPR curve. After promoter is introduced in the Fe/C catalyst, the H_2 reduction process is clearly enhanced in terms of the peak shift towards a low temperature (404 °C for Fe/C-Chem and 424 °C for Fe/C-Bio), suggesting the promotional effect on the decomposition of humboldtine of the electronic promoters (K, Mg, Ca). Totally, the reduction process with H_2 at 400 °C before reactions is enhanced on bio- and chem-promoted catalysts.

The ^{57}Fe Mössbauer spectra of the catalysts in Fig. 3 further disclose the formation and transformation of active phases in the various stages from fresh, reduced, to used catalysts. The detailed composition and comparison of different phases are also listed in Supplementary Table 7 and Supplementary Fig. 8. As indicated above, iron species in the fresh Fe/C-Bio are present in terms of humboldtine. After reduction at 400 °C in hydrogen, the Fe/C catalyst without promoters is composed of metal iron (76%), χ-Fe_5C_2 (8.7%), and super-paramagnetism (spm) Fe^{3+} (15.3%). More interestingly, the composition is greatly changed after biopromoters are physically introduced in the catalyst. The content of χ-Fe_5C_2 reaches as high as 64.5%, accompanied by a sharply decrease of metal iron to 9.8%, demonstrating an obviously promotional effect of biopromoters on the carbinization of iron in the reduction process. The content of χ-Fe_5C_2 further climbes to a higher value of 87.2%, while no metal iron is observed in the Fe/C-Bio catalyst after reaction, suggesting that the metal iron is further carbonized after exposing in the atmosphere of CO_2 and H_2 as feedstocks.

In comparison, the content of χ-Fe_5C_2 for the used Fe/C catalyst with chemical promoters is only 34.1%, and a large amount of metal iron (30.1%) cannot be completely carbonized in the catalyst. These findings clearly show that the superiority of biopromoters in promoting the formation of iron carbides as compared to chemical promoters, and the above promotional effect primarily occurs in the reduction process prior to catalytic reactions. In spite of similar chemical composition for the Fe/C catalysts with chemical and biological promoters, the unique synergistic catalytic role probably exists in the bio-promoted catalyst.

X-ray photoelectron spectroscopy (XPS) was applied to investigate the phase composition and content of surface species. The binding energy peaks at 711.4, 710.3, and 708.5 eV in the Fe2p spectrum are correspondingly ascribed to Fe^{III}, Fe^{II}, and Fe-C (Fig. 4a)[32]. As for C1s spectrum, the binding energy peaks ca. 281.0, 282.0, and 284.8 eV are correspondingly contributed to C-Fe, C = C, and C–C bonds (Fig. 4b)[21]. Clearly, the content of Fe-C in the Fe2p spectrum is significantly enhanced with the addition of biopromoters, in accordance with that of C-Fe suggested in the C1s spectrum, further indicating the existence of biopromoters aggravates the carbonization process of iron species. The calculated surface content of iron carbides on the used Fe/C-Bio catalyst is increased to 48% from 19% for the reduced catalyst. Both contents are lower than those from the previous MES analysis, reflecting that the iron carbides are more favorable to be formed on catalyst bulk.

More importantly, it is necessary to study the content of K and carbides in catalysts surface in view of the fact that K influences the olefins hydrogenation as well as carbides affects the selectivity of heavy hydrocarbons. According to the results of XPS surface analysis, the surface atom ratio of K/Fe in the reduced Fe/C-Bio reaches 1.4, far higher than its stoichiometry in bulk (0.3), and the value further climbs to as high as 2.7 after reaction, nearly double of that before reaction, suggesting the obvious K enrichment on catalyst surface in the reduction and reaction process[33, 34]. Simultaneously, the K content in bulk of the fresh, used for 6 h and used for 100 h Fe/C-Bio catalyst is not obviously changed a lot (Supplementary Tables 2 and 8).

However, the surface K/Fe ratio in the used Fe/C-Chem catalyst is merely 0.4, close to the theoretical value. K was more easily to be enriched on the surface of the bio-promoted catalyst rather than chemical-promoted catalysts. It seems that K in biopromoters has stronger migration ability than chemical promoters, probably resulting from the unique synergistic effect between K with other elements. The migration ability could improve its contact interface between active phases and electronic promoter.

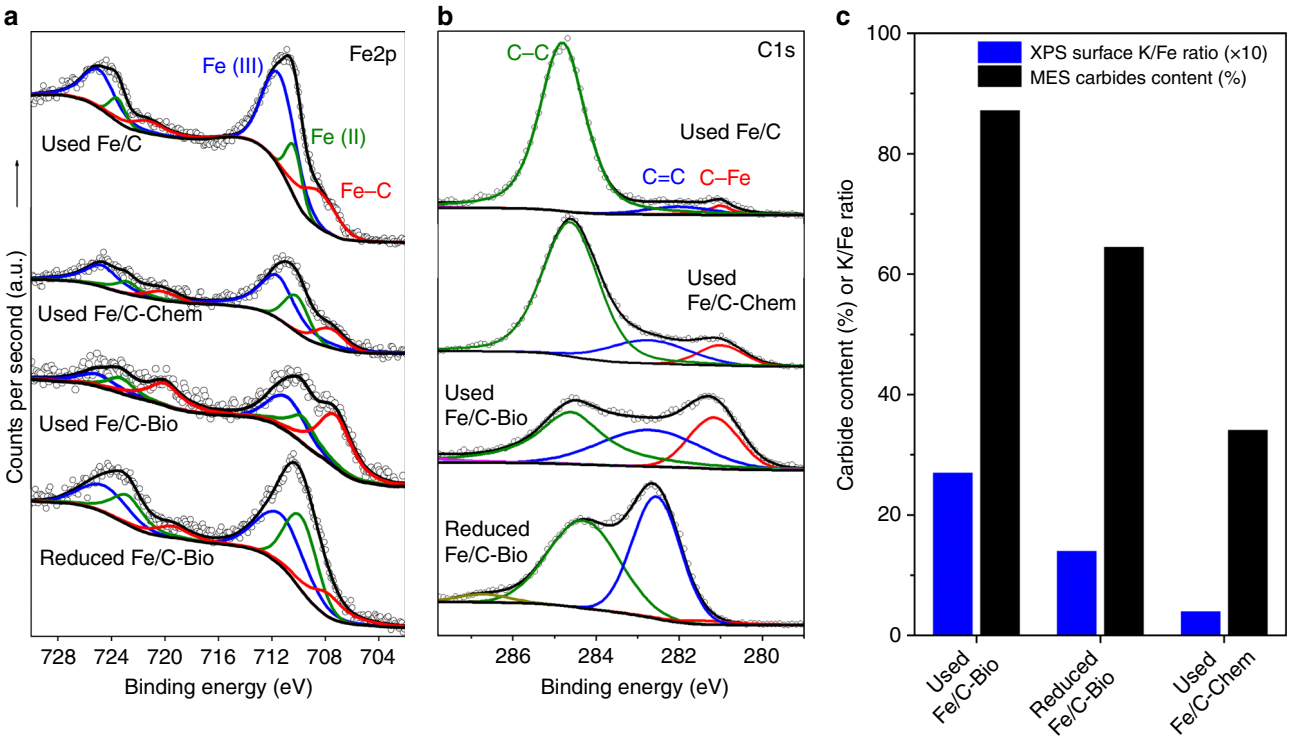

Fig. 4 Surface analysis of different catalysts. Fe2p (**a**) and C1s (**b**) XPS spectra of used Fe/C, Fe/C-Bio, Fe/C-Chem, and reduced Fe/C-Bio. **c** The relationship between surface K/Fe ratio and carbides content in the catalysts. The carbides content and K/Fe ratio on surface is derived from XPS analysis, and the carbides content in bulk is calculated from ^{57}Fe Mössbauer spectra analysis

A relationship between the surface K/Fe ratio and the content of iron carbides can be accordingly established as shown in Fig. 4c. Under the experiment conditions in this work, the content of iron carbides gradually increase with the increase of the surface K/Fe ratio. However, there must be a optimized value for the surface K/Fe ratio as the excessive K may cover the active iron sites. In our case, surface enriched K sharply promotes the formation of more carbides than unpromoted and chemical-promoted ones, which is in accordance with XRD patterns, MES analysis, XPS spectra as well as other reports[35]. In addition, the carbides content from XPS for the used Fe/C-Chem is almost unchanged compared with the used Fe/C, suggesting surface enriched K is more effective than bulk dispersed K. The vast amount of carbides produces higher α-value, improving chain growth probability.

It is imperative to investigate the secondary hydrogenation ability of olefins, which severely influence olefin selectivity in hydrocarbons, thus the in situ pulse experiments of propene over reacted Fe/C, Fe/C-Chem, and Fe/C-Bio catalysts were further employed. Figure 5 shows that more propene was converted into propane on the unpromoted Fe/C compared to the case of Fe/C-Bio and Fe/C-Chem when isometric propene was pulsed into the reactor. It indicates the addition of promoters will suppress the hydrogenation of olefins, and biopromoters-modified iron catalyst shows higher habitation ability towards olefins hydrogenation than chemical promoters. As shown in Table 1, the selectivity of olefins over Fe/C-Bio (72 %) is the highest, followed by Fe/C-Chem (53.1 %), and Fe/C presented an inferior selectivity of olefins (21.2 %), which is in accordance with the results of pulse experiments.

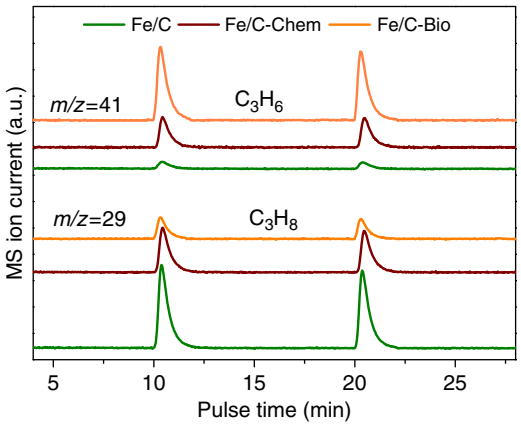

Fig. 5 Characterization of hydrogenation ability by the pulse experiment of propylene. Before reaction, the catalysts (100 mg) were in situ reduced with H_2 (30 ml min^{-1}, 400 °C) and remained 90 min, then reacted in feed gas (20 ml min^{-1}, 0.1 MPa, 320 °C) for 30 min. After re-switching to a flow of H_2 (20 ml min^{-1}), propene of 120 μl was pulsed into the reactor with a certain time interval and detected by mass spectrometry

Discussion

LAOs are known to be the primary intermediates of C–C coupling. After LAOs are formed, they can reabsorb on the active sites and undergo secondary reactions. Weaker hydrogenation ability of olefins over Fe/C-Bio is beneficial to the production of α-olefins. Ethylene, propylene, and α-olefins with low carbon number undergo oligomerization reactions over carbides to form more long-chain LAOs. A well match between the high activity of C–C coupling and weak hydrogenation ability is responsible for the excellent catalytic performance with a high C_{4-18} alkenes selectivity of 50.3 as well as 80% LAO in C_{4-18} alkenes. The detailed reaction scheme in combination with experimental and characterization results is depicted in Fig. 6. Thus, it is possible to tune the selectivity of linear olefins by changing the activity of C–C coupling and hydrogenation ability of

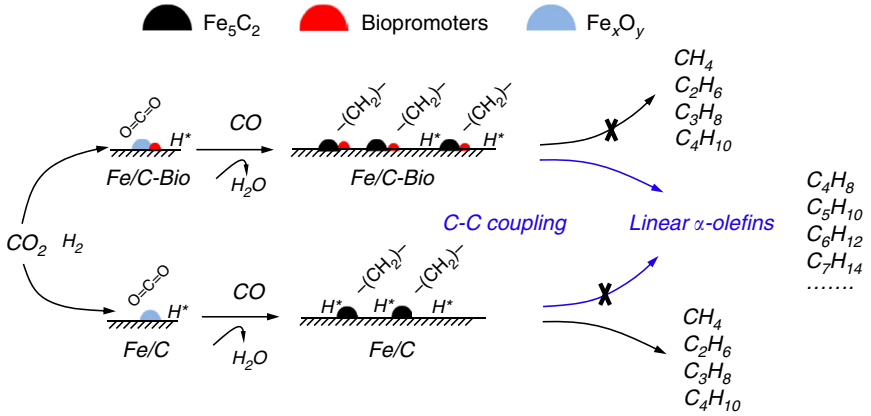

Fig. 6 Reaction scheme for CO_2 hydrogenation to LAO. The existences of biopromoters weaken secondary hydrogenation of olefins and strengthen the reaction activity of C–C coupling

active sites. Although the addition of chemical promoters weakens the secondary hydrogenation reaction as well, it does not sharply raise the content of carbides on catalyst surface as well as the interface between carbides and promoters. Therefore, the catalytic performance via biopromoters addition cannot be completely simulated by a chemical addition route of multiple promoters. Enough content of carbides and weak alkenes hydrogenation ability are indispensable for heavy olefins formation.

It is noteworthy that the formation of enough content of carbides in the H_2 reduction stage prior to catalytic reactions is more important to achieve superior performance in LAO production reactions instead of the in situ carbonization process, as reflected by the carbides content from the previous characterization analysis. The similar superior performance in LAO production with CO and H_2 as feedstocks (Supplementary Table 4) also demonstrates it. In an additional case for comparison, the bare Fe catalyst is prepared without glucose in raw materials under the same hydrothermal conditions as Fe/C. However, no iron carbides are formed in this bare Fe catalyst after the pretreatment under the same H_2 reduction condition as others. Thus, it shows the lowest conversion and LAO selectivity among all self-made iron-based catalysts.

In summary, although the addition of K as a chemical promotor suppressed alkene hydrogenation, the activity of C–C coupling is lower than that of Fe/C-Bio owing to the lack of carbide content. K derived from biopromoters shows stronger migration ability than chemical promoters during the CO_2 hydrogenation process. These surface enriched K ions could promote the formation of carbides and further enhance the activity of C–C coupling. Besides, the surface-enriched K suppresses the hydrogenation of alkenes and leads to more formation of alkenes. The optimal content and existing form of mineral elements in biomass are promising for improving the performance of heterogeneous catalytic CO_2 hydrogenation when these promoters were added into iron catalysts. Thus, this design of biopromoters-modified catalyst provides a new strategy for selective hydrogenation of CO_2 into high value-added products, and sheds a light on the rational design of high efficiently catalysts referenced from biocatalysis in nature.

Methods

Catalyst preparation. To attain mineral element-rich powder, CC was calcined under 500 °C and remains 180 min in flowing air. The element content of pretreated CC ash is shown in Supplementary Table 1. As for the preparation of Fe/C, glucose and iron nitrate was dispersed in the deionized water solution. After vigorous stirring of 1 h, the derived turbid liquid was transferred into a 100 ml capacity Teflon-lined stainless steel autoclave, followed by one-pot hydrothermal treatment at 150 °C for 24 h. Obtained products were washed and filtered off for five times with distilled water and ethanol successively. Finally, products were dried in crucibles at 120 °C overnight, denoted as Fe/C.

The promoter(s)-modified Fe/C catalysts were fabricated by simple physical mixing the corresponding promoter(s) and Fe/C powder. The raw material for each promoter in the promoted Fe/C catalyst is KCl, MgO, $CaCO_3$, and SiO_2 (Fe/C-K, Fe/C-Mg, Fe/C-Ca, and Fe/C-Si catalysts just contain single corresponding chemical promoter; Fe/C-Chem catalysts contain four chemical promoters; Fe/C-Bio stands for biopromoters-modified Fe/C catalysts). The addition of each chemical element is equal to the value existed in the content of biopromoters-modified Fe/C-Bio. For example, Fe/C-Bio was fabricated via physical mixing 0.15 g prepared CC ash and 1.0 g Fe/C powder, following pelleting the mixtures with a 20–40 mesh size.

To remove the soluble KCl existed in biopromoters, 0.15 g biopromoters were washed for five times with 1.5 l deionized water (noted as CC-W). The pretreated CC-W was mixed with Fe/C and marked as Fe/C-Bio-W.

As for the Fe/C-K, Ca, Mg, S catalyst, the introduction form of S element was iron sulfate ($FeSO_4$).

Catalyst characterization. The element content of pretreated CC ash was tested by a Philips Magix-601 wave-dispersive X-Ray Fluorescence (WD-XRF) and a PerkinElmer 7300DV Inductively Coupled Plasma Optical Emission Spectrometer (ICP-OES).

XRD spectra were obtained on a PANalytical X'pert Pro diffractometer equipped with Cu-Kα (40 kV, 40 mA) irradiation.

Scanning electron microscopy (SEM) images were taken by a JSM-7800F microscope operated at an accelerating voltage of 1.5 kV, which were used to obtain the surface morphology and elemental composition of the prepared catalysts. SEM with dispersive spectroscopy (SEM-EDS) was used to attain the elemental maps.

TEM images were obtained by using a JEOL JEM-2000EX (120 kV) microscope.

The XPS measurements were conducted on an ESCALAB 250Xi equipped with Al Kα radiation.

The ^{57}Fe Mössbauer spectra (MES) of the catalysts were recorded at room temperature using a Topologic 500A spectrometer and a proportional counter. ^{57}Co (Rh) moving in a constant acceleration mode was used as a radioactive source. Magnetic hyperfine field was calibrated with the 330-kOe field of α-Fe at ambient temperature.

The hydrogen temperature-programmed reduction (H_2-TPR) experiments were carried out in a home-made apparatus. A 10 mg of sample was in situ treated by an Ar stream (30 ml min^{-1}) at 400 °C for 30 min. After cooling down to room temperature, the sample was heated to 1000 °C with a temperature ramp of 10 °C min^{-1} in a 5% H_2/95% ar flow (30 ml min^{-1}). The hydrogen concentration in the effluent was continuously monitored by a TCD detector.

Catalytic activity test. The prepared catalysts were *in situ* reduced at 400 °C for 10 h using H_2 (40 ml min^{-1}, atmospheric pressure) prior to CO_2 hydrogenation tests. Briefly, CO_2 hydrogenation reaction was performed with a continuous flowing fixed-bed reactor from feed gas (CO_2: 24 v%, H_2: 72 v%, N_2: 4 v%). An ice trap of n-octane as solvent was equipped to capture the heavy hydrocarbons in the effluent. Reaction conditions were 320 °C, 1.0 MPa, and $W_{catalyst}/F = 10$ g h mol^{-1}. Gas products were analyzed by two on-line gas chromatographs, one of which employed an active charcoal column equipped with a thermal conductivity detector (Shimadzu, GC-8A). Another used a capillary column and a flame ionization detector (Agilent Technologies, 7890 A) to analyze light hydrocarbons. Liquid products from the ice trap were analyzed by an off-line gas chromatograph using a flame ionization detector (Agilent Technologies, 7890A).

Data availability. The data supporting the findings of this study are available within the article and its Supplementary Information files. All other relevant source data are available from the corresponding author upon reasonable request.

Received: 11 January 2018 Accepted: 23 January 2018
Published online: 22 March 2018

References

1. Porosoff, M. D., Yan, B. & Chen, J. G. Catalytic reduction of CO_2 by H_2 for synthesis of CO, methanol and hydrocarbons: challenges and opportunities. *Energy Environ. Sci.* **9**, 62–73 (2016).
2. Wang, W., Wang, S., Ma, X. & Gong, J. Recent advances in catalytic hydrogenation of carbon dioxide. *Chem. Soc. Rev.* **40**, 3703–3727 (2011).
3. Owen, R. E. et al. Effect of support of Co-Na-Mo catalysts on the direct conversion of CO_2 to hydrocarbons. *J. CO2 Util.* **16**, 97–103 (2016).
4. Visconti, C. G. et al. CO_2 hydrogenation to lower olefins on a high surface area K-promoted bulk Fe-catalyst. *Appl. Catal. B* **200**, 530–542 (2017).
5. Xu, L. et al. The promotions of MnO and K_2O to Fe/silicalite-2 catalyst for the production of light alkenes from CO_2 hydrogenation. *Appl. Catal. A* **173**, 19–25 (1998).
6. Satthawong, R., Koizumi, N., Song, C. & Prasassarakich, P. Light olefin synthesis from CO_2 hydrogenation over K-promoted Fe-Co bimetallic catalysts. *Catal. Today* **251**, 34–40 (2015).
7. Choi, P. H., Jun, K. W., Lee, S. J., Choi, M. J. & Lee, K. W. Hydrogenation of carbon dioxide over alumina supported Fe-K catalysts. *Catal. Lett.* **40**, 115–118 (1996).
8. Zhang, J. et al. Selective formation of light olefins from CO_2 hydrogenation over Fe-Zn-K catalysts. *J. CO2 Util.* **12**, 95–100 (2015).
9. Wei, J. et al. New insights into the effect of sodium on Fe_3O_4-based nanocatalysts for CO_2 hydrogenation to light olefins. *Catal. Sci. Technol.* **6**, 4786–4793 (2016).
10. Skupinska, J. Oligomerization of α-olefins to higher oligomers. *Chem. Rev.* **91**, 613–648 (1991).
11. Lu, Y. et al. Fischer–Tropsch synthesis of olefin-rich liquid hydrocarbons from biomass-derived syngas over carbon-encapsulated iron carbide/iron nanoparticles catalyst. *Fuel* **193**, 369–384 (2017).
12. Small, B. L. & Brookhart, M. Iron-based catalysts with exceptionally high activities and selectivities for oligomerization of ethylene to linear α-olefins. *J. Am. Chem. Soc.* **120**, 7143–7144 (1998).
13. Keim, W. Oligomerization of ethylene to alpha-olefins: discovery and development of the shell higher olefin process (SHOP). *Angew. Chem. Int. Ed.* **52**, 12492–12496 (2013).
14. Li, C., Sayaka, I., Chisato, F. & Fujimoto, K. Development of high performance graphite-supported iron catalyst for Fischer–Tropsch synthesis. *Appl. Catal. A* **509**, 123–129 (2016).
15. Zhai, P. et al. Highly tunable selectivity for syngas-derived alkenes over Zinc and Sodium-modulated Fe_5C_2 catalyst. *Angew. Chem. Int. Ed.* **55**, 1–7 (2016).
16. Satthawong, R., Koizumi, N., Song, C. & Prasassarakich, P. Bimetallic Fe-Co catalysts for CO_2 hydrogenation to higher hydrocarbons. *J. CO2 Util.* **3–4**, 102–106 (2013).
17. Satthawong, R., Koizumi, N., Song, C. & Prasassarakich, P. Comparative study on CO_2 hydrogenation to higher hydrocarbons over Fe-based bimetallic catalysts. *Top. Catal.* **57**, 588–594 (2013).
18. Choi, Y. H. et al. Carbon dioxide Fischer-Tropsch synthesis: a new path to carbon-neutral fuels. *Appl. Catal. B* **202**, 605–610 (2017).
19. Wei, J. et al. Directly converting CO_2 into a gasoline fuel. *Nat. Commun.* **8**, 15174 (2017).
20. Gao, P. et al. Direct conversion of CO_2 into liquid fuels with high selectivity over a bifunctional catalyst. *Nat. Chem.* **9**, 1019–1024 (2017).
21. Sun, J. et al. Green synthesis of rice bran microsphere catalysts containing natural biopromoters. *ChemCatChem* **7**, 1642–1645 (2015).
22. Yu, G. et al. FexOy@C spheres as an excellent catalyst for Fischer-Tropsch synthesis. *J. Am. Chem. Soc.* **132**, 935–937 (2010).
23. Sun, B., Xu, K., Nguyen, L., Qiao, M. & Tao, F. F. Preparation and catalysis of carbon-supported iron catalysts for Fischer-Tropsch synthesis. *ChemCatChem* **4**, 1498–1511 (2012).
24. Torres Galvis, H. M. et al. Supported iron nanoparticles as catalysts for sustainable production of lower olefins. *Science* **335**, 835–838 (2012).
25. Amoyal, M., Vidruk-Nehemya, R., Landau, M. V. & Herskowitz, M. Effect of potassium on the active phases of Fe catalysts for carbon dioxide conversion to liquid fuels through hydrogenation. *J. Catal.* **348**, 29–39 (2017).
26. Pour, A. N. et al. Effect of Mg, La and Ca promoters on the structure and catalytic behavior of iron-based catalysts in Fischer-Tropsch synthesis. *Appl. Catal. A* **348**, 201–208 (2008).
27. Pham, T. H. et al. Insights into Hägg iron-carbide-catalyzed Fischer–Tropsch synthesis: suppression of CH_4 formation and enhancement of C–C coupling on χ-Fe_5C_2 (510). *ACS Catal.* **5**, 2203–2208 (2015).
28. Rivera de la Cruz, J. G., Sabbe, M. K. & Reyniers, M.-F. First principle study on the adsorption of hydrocarbon chains involved in Fischer–Tropsch synthesis over iron carbides. *J. Phys. Chem. C* **121**, 25052–25063 (2017).
29. Carles, V., Alphonse, P., Tailhades, P. & Rousset, A. Study of thermal decomposition of $FeC_2O_4{\cdot}2H_2O$ under hydrogen. *Thermochim. Acta* **334**, 107–113 (1999).
30. Torres Galvis, H. M. et al. Iron particle size effects for direct production of lower olefins from synthesis gas. *J. Am. Chem. Soc.* **134**, 16207–16215 (2012).
31. Yang, C., Zhao, H., Hou, Y. & Ma, D. Fe_5C_2 nanoparticles: a facile bromide-induced synthesis and as an active phase for Fischer-Tropsch synthesis. *J. Am. Chem. Soc.* **134**, 15814–15821 (2012).
32. Yamashita, T. & Hayes, P. Analysis of XPS spectra of Fe^{2+} and Fe^{3+} ions in oxide materials. *Appl. Surf. Sci.* **254**, 2441–2449 (2008).
33. Sai Prasad, P. S., Bae, J. W., Jun, K.-W. & Lee, K.-W. Fischer-Tropsch synthesis by carbon dioxide hydrogenation on Fe-based catalysts. *Catal. Surv. Asia* **12**, 170–183 (2008).
34. Li, J. et al. Alkalis in iron-based Fischer-Tropsch synthesis catalysts: distribution, migration and promotion. *J. Chem. Technol. Biotechnol.* **92**, 1472–1480 (2017).
35. Zhenya, Y., Weiping, D., Qinghong, Z. & Ye, W. Hydrogenation of carbon dioxide to light olefins over non-supported iron catalyst. *Chin. J. Catal.* **34**, 956–963 (2013).

Acknowledgements

J.S. thanks the support of the National Natural Science Foundation of China (21503215, 91745107), the Hundred-Talent Program of Dalian Institute of Chemical Physics and the Youth Innovation Promotion Association of Chinese Academy of Sciences (CAS).

Author contributions

L.G., J.S., and Q.G. conceived the research, designed the experiments, and wrote the manuscript. L.G. synthesized and characterized the catalysts. L.G., J.W., X.J., Z.W., and Y.R. performed the reaction testing. All the authors contributed to analysis and discussion on the data. Q.G., J.S., and H.X. supervised the whole project.

Additional information

Supplementary information accompanies this paper at https://doi.org/10.1038/s42004-018-0012-4.

Competing interests: The authors declare no competing interests.

Reprints and permission information is available online at http://npg.nature.com/reprintsandpermissions/

Publisher's note: Springer Nature remains neutral with regard to jurisdictional claims in published maps and institutional affiliations.